◆ Human Brain Mapping 30:711–724 (2009) ◆

Source-Based Morphometry: The Use of Independent Component Analysis to Identify Gray Matter Differences With Application to Schizophrenia

Lai Xu,[1,2] Karyn M. Groth,[3] Godfrey Pearlson,[3,4] David J. Schretlen,[5] and Vince D. Calhoun[1,2,3,4]*

[1]*The MIND Institute, Albuquerque, New Mexico*
[2]*Department of ECE, University of New Mexico, Albuquerque, New Mexico*
[3]*Olin Neuropsychiatry Research Center, Institute of Living, Hartford, Connecticut*
[4]*Department of Psychiatry, Yale University School of Medicine, New Haven, Connecticut*
[5]*Department of Psychiatry, Johns Hopkins University School of Medicine, Baltimore, Maryland*

Abstract: We present a multivariate alternative to the voxel-based morphometry (VBM) approach called source-based morphometry (SBM), to study gray matter differences between patients and healthy controls. The SBM approach begins with the same preprocessing procedures as VBM. Next, independent component analysis is used to identify naturally grouping, maximally independent sources. Finally, statistical analyses are used to determine the significant sources and their relationship to other variables. The identified "source networks," groups of spatially distinct regions with common covariation among subjects, provide information about localization of gray matter changes and their variation among individuals. In this study, we first compared VBM and SBM via a simulation and then applied both methods to real data obtained from 120 chronic schizophrenia patients and 120 healthy controls. SBM identified five gray matter sources as significantly associated with schizophrenia. These included sources in the bilateral temporal lobes, thalamus, basal ganglia, parietal lobe, and frontotemporal regions. None of these showed an effect of sex. Two sources in the bilateral temporal and parietal lobes showed age-related reductions. The most significant source of schizophrenia-related gray matter changes identified by SBM occurred in the bilateral temporal lobe, while the most significant change found by VBM occurred in the thalamus. The SBM approach found changes not identified by VBM in basal ganglia, parietal, and occipital lobe. These findings show that SBM is a multivariate alternative to VBM, with wide applicability to studying changes in brain structure. *Hum Brain Mapp 30:711–724, 2009.* © 2008 Wiley-Liss, Inc.

Key words: schizophrenia; structural MRI; source-based morphometry; independent component analysis; voxel-based morphometry

Contract grant sponsor: National Institute of Health; Contract grant numbers: 1 R01 EB 000840, 1 R01 EB 005846, 2 RO1 MH43775, 5 RO1 MH52886; Contract grant sponsor: NARSAD Distinguished Investigator Award.

*Correspondence to: Vince D. Calhoun, Ph.D., The MIND Institute, 1101 Yale Boulevard, Albuquerque, NM 87131.
E-mail: vcalhoun@unm.edu

Received for publication 19 July 2007; Revised 19 November 2007; Accepted 17 December 2007
DOI: 10.1002/hbm.20540
Published online 11 February 2008 in Wiley InterScience (www.interscience.wiley.com).

© 2008 Wiley-Liss, Inc.

INTRODUCTION

Structural magnetic resonance imaging (sMRI) is a useful tool for detecting differences in brain morphometry. It has been used to study various illnesses including schizophrenia and Alzheimer's disease. A common approach to study changes in brain structure is to manually or automatically separate the brain into regions of interest (ROI) and to compute volumes difference between groups. Such studies are important and needed; however, a limitation of this approach is they only provide information about brain structures or regions that can be clearly defined anatomically. More recently, investigators have begun using voxel-based morphometry (VBM) to identify group differences throughout the brain simultaneously [Good et al., 2001]. This method is fully automated and can compare changes in voxels throughout the whole brain via a statistical map. However, since VBM is a univariate method, it does not utilize any information about the relationships among voxels. In addition, it will only detect voxels for which a specific predicted effect is present (typically, a mean difference between two groups). In contrast, a multivariate, data-driven approach can provide a way to pool information across different voxels as well as identify unpredicted patterns. The voxels that carry similar information will group to a set of regions which we call a "network." This network exhibits intersubject covariance and differences between groups.

Independent component analysis (ICA) is a popular statistical and computational technique for biomedical signal analysis. The biomedical signals that we can measure are often mixtures of signals from different underlying "sources," including both noise or signals of interest. ICA works by decomposing the mixed signals into maximally independent components. ICA has shown considerable promise for the analysis of fMRI [Calhoun and Adali, 2006] and EEG data [Makeig et al., 1997] and also for segmenting the gray matter and white matter in sMRI [Nakai et al., 2004]. Here we propose the use of ICA to extract maximally spatially independent sources revealing patterns of variation that occur in sMRI images and to identify sMRI differences between patients and healthy controls. We hypothesized that a small number of sources in the brain would show differences between patients and healthy controls. Under this assumption, we can apply ICA to the preprocessed sMRI images, identify the sources, and perform statistical analysis to identify which sources distinguish patients from healthy controls. We refer to this straightforward but effective approach as source-based morphometry (SBM).

Schizophrenia is a well-studied mental illness in which many abnormal brain regions have been identified [Pearlson and Marsh, 1999; Shenton et al., 2001]. However, it is not clear from previous approaches how these different brain regions might be subdivided into naturally grouped circuits. Therefore, we applied this novel SBM approach to data collected from patients with schizophrenia and healthy controls. In principle, SBM is a proper approach to studying group differences, because it does not require prior definition of the ROIs. And being multivariate, SBM utilizes the spatial information between voxels to identify multiple grouped sources in a natural manner. These spatially distinct sources also covary between subjects in a particular manner. We expect SBM may well be useful as a tool for studying schizophrenia.

In this paper, we first provide a brief overview of SBM, including a simulation comparing SBM with the commonly used VBM approach. The aim of this overview is to introduce the concept of SBM. Next, we describe in detail the SBM approach and demonstrate the use of SBM on gray matter segmentation images from a group of healthy controls and patients with schizophrenia. Because of the assumption of linear mixing, each of the maximally independent components (sources) identified by ICA linearly covaries in gray matter concentration from individual to individual. We then determine the sources that differed significantly between the two groups in order to study structural changes occurring in patients with schizophrenia versus healthy controls. A comparison of the identified sources with VBM is also performed.

SOURCE-BASED MORPHOMETRY OVERVIEW

SBM requires three fundamental steps: image preprocessing, ICA, and statistical analysis (see Fig. 1). The raw images are first preprocessed identically to VBM [Ashburner and Friston, 1997, 2000; Good et al., 2001]. Then ICA is used to separate the preprocessed images to derive the spatially independent components. Finally, we subject the components to a statistical analysis to determine the significant sources, remove noise, and analyze the effect of other factors.

As shown in Figure 1, the main difference between SBM and VBM is the introduction of ICA, which is used to identify natural groupings in the data. This difference can be clarified by a simple simulation (see Fig. 2). First, we generated a circular region with a radius of 25 voxels and a standard deviation of six voxels. Two sources were simulated, as shown in Figure 2a,b. Every source consisted of two separate circular regions; the upper region of Source 1 and the upper region of Source 2 are partially overlapping. Using these sources, we generate 100 images that represent the gray matter images of healthy controls (see Fig. 2c) and 100 images that represent the gray matter images of schizophrenia patients (see Fig. 2d). For healthy controls, the intensities of Source 1 were uniformly distributed between 70% and 90% of the original source intensity, and the intensities of Source 2 were uniformly distributed between 10% and 60% of the original source intensity. For patients, the intensities of Source 1 were uniformly distributed between 40% and 60% of the original source intensity and the intensities of Source 2 were uniformly distributed between 10% and 60% of the original source intensity.

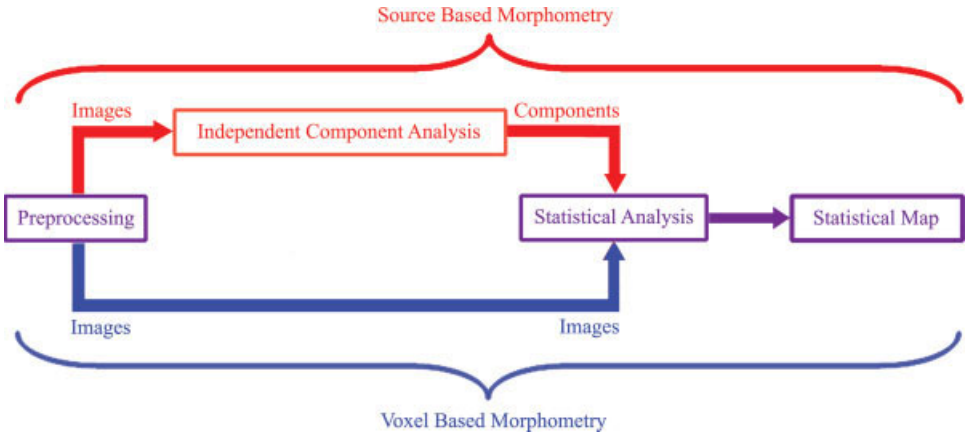

Figure 1.

The approach difference between source-based morphometry and voxel-based morphometry. [Color figure can be viewed in the online issue, which is available at www.interscience.wiley.com.]

Therefore, the regions associated with Source 1 had higher mean intensity in the images of healthy controls than in the images of patients, representing the gray matter reduction in schizophrenia. Likewise, the mean of intensity of Source 2 in the patient images and healthy control images are the same, simulating gray matter regions that are not affected by illness. Gaussian noise was then added to the 200 images. SBM and VBM were carried out on these 200 images separately in order to evaluate their performance. Figure 2e,f show the SBM result thresholded at $|Z| > 3.0$ and Figure 2g shows the VBM result at the same threshold (we used a Z threshold to display the images, to provide a fair comparison of the two). We can also compare the t values from the voxels in VBM and the mixing matrix in SBM. The t values for the SBM results are 13.70 (for Source 1) and -1.46 (for Source 2). The maximal t value of VBM result is 9.99. It is clear that SBM can effectively separate the two sources and the Gaussian noise, while VBM can identify only voxels that match the prediction (in this case, a difference between groups). In addition, VBM appears to have less sensitivity when there are overlapping regions, some of which show a group difference and some of which do not. This is where the multivariate aspect of SBM also provides an advantage, since SBM can assign a single voxel to multiple sources. Since we have the ground truth available in the simulation, we also computed ROC curves for both SBM and VBM by varying the threshold $|Z|$ (see Fig. 2h), hence allowing us to clearly identify the performance of both approaches. To compute the performance, the percentage of voxels within both the detected regions and ground truth regions was used as a measure of the sensitivity, and the percentage of voxels outside both the detected regions and ground truth regions was used as a measure of specificity. From this ROC curve, it is clear that SBM was showing better sensitivity and specificity (the area under the ROC curve is larger) than VBM for the example shown.

We next describe an application of SBM to real sMRI data collected from healthy controls and patients with schizophrenia.

SUBJECTS AND METHODS

Participants

One hundred and twenty participants with schizophrenia (51 females; mean age = 42.1; SD = 12.9; range, 20–81) and 120 matched healthy controls (65 females; mean age = 42.8; SD = 16.57; range, 18–78) were scanned at Johns Hopkins University. Exclusion criteria for all participants included a history of overt brain disease, mental retardation, head injury with loss of consciousness for greater than 30 min, or a diagnosis of substance abuse within the last year or lifetime dependence. Healthy participants were recruited using random-digit dialing as part of Phase 1 of the Johns Hopkins aging, brain, and cognition study. All healthy controls were screened to ensure they were free from DSM-III-R/DSM-IV Axis I or Axis II psychopathology (SCID) [First et al., 1997; Spitzer et al., 1989]. Patients met criteria for schizophrenia in the DSM-IV on the basis of a SCID diagnosis and review of the case file. All patients with schizophrenia were stable and taking antipsychotic medications (the exact medication information was not available for these data).

Imaging Parameters

Whole brain sMRIs were obtained on a single 1.5-T scanner (Signa; GE Medical Systems, Milwaukee, WI). The whole brain was evaluated in the coronal plane using a "spoiled" SPGR 3D imaging sequence, with the following imaging parameters: 35 ms TR, 5 ms TE, 45° flip angle, 1 excitation, 1.5-mm slice thickness, 24-cm field of view, and a matrix size of 256 × 256.

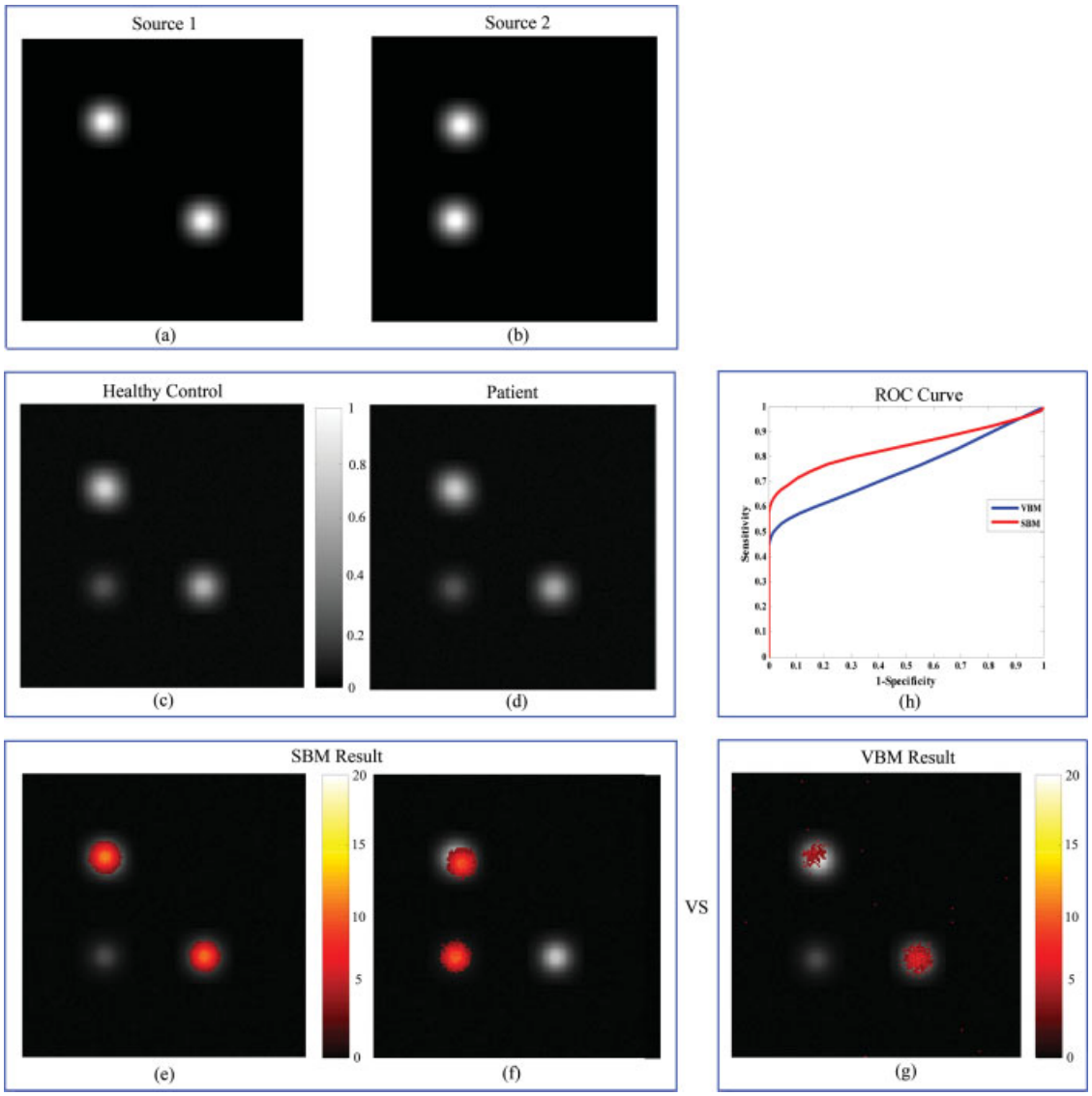

Figure 2.

Simulation for SBM vs. VBM. (**a**) Source 1. (**b**) Source 2. (**c**) Image represents the gray matter of the healthy control. (**d**) Image represents the gray matter of the schizophrenia patient (**e**,**f**). SBM result. (**g**) VBM result. (**h**) ROC curve.

Image Preprocessing

The images were preprocessed using the preprocessing steps used for VBM [Ashburner and Friston, 1997, 2000; Good et al., 2001] and employed the Matlab program SPM5 (Statistical Parametric Mapping, developed by the Welcome Institute, London, UK). Images were first roughly normalized using a 12-parameter affine model to the 152 average T_1 Montreal Neurological Institute (MNI) template. Normalized images were then interpolated to voxel dimensions of $1.5 \times 1.5 \times 1.5$ mm^3 and segmented into gray, white, and cerebrospinal fluid compartments using a modified mixture model cluster analysis technique, with a correction for image intensity nonuniformity [Ashburner and Friston, 1997]. The gray matter images were then smoothed with 12-mm full width at half-maximum Gaussian kernel. Each voxel in a smoothed image contains the averaged partial volume of gray matter from around and within the selected voxel, which contains gray matter concentration, a value ranging from 0 (no gray matter) to 1 (all gray matter).

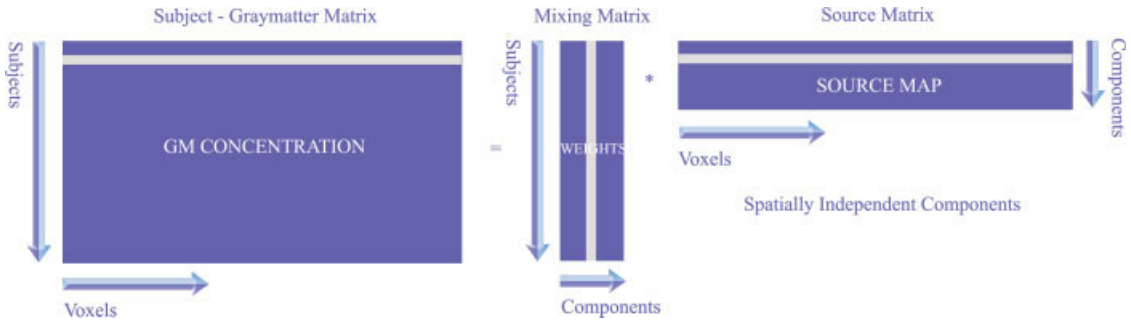

Figure 3.

ICA model in which the subject-by-gray matter matrix was decomposed into mixing matrix and source matrix. [Color figure can be viewed in the online issue, which is available at www.interscience.wiley.com.]

Component Estimation

Before doing independent component analysis, we needed to determine how many components should be extracted from the gray matter images. We used an information-theoretic approach to solve this problem. First, we uniformly subsampled the gray matter images until the estimated entropy rate equaled the entropy rate of an independent and identically distributed (i.i.d.) Gaussian random process of the same variance and data length. This subsampling is based on the entropy rate matching principle, which makes the entropy of the images reach an upper bound and generated an i.i.d. image set for the component estimation [Li et al., 2007].

Next, we estimated the number of components using the well-known Akaike's information criterion (AIC) ([Akaike, 1974], which is a standard information-theoretic method for estimating the number of components from the aggregate data set [Calhoun et al., 2001]. The equation of this method is given as follows,

$$\mathrm{AIC}(k) = -2 \times L(k) + 2 \times \mathrm{d}f(k) \tag{1}$$

The estimate for the number of sources is determined from the minima of the above function AIC(k) with respect to k, where k is the number of components to be estimated, $L(k)$ is the maximum log-likelihood of the gray images based on the parameter set, d$f(k)$ is a penalty for model complexity given by the total number of free parameters. The maximum log-likelihood [Karhunen et al., 1997; Wax and Kailath, 1985] is given by

$$L(k) = \frac{N}{2}(p-k)\ \log\left(\frac{(\lambda_{k+1}\ldots\lambda_p)^{\frac{1}{p-k}}}{\frac{1}{p-k}(\lambda_{k+1}\ldots\lambda_p)}\right) \tag{2}$$

where N is the number of voxels within one image after subsampling, p is the number of gray matter images (sample size), λ_i s are the eigenvalues of the covariance matrix of the samples. The number of free parameters is given by

$$\mathrm{d}f(k) = 1 + pk - \frac{1}{2}k(k-1) \tag{3}$$

Thus, the component number k can be estimated from the 240 gray matter images. This approach allowed us to estimate the component number using a principled approach rather than arbitrarily selecting the number of components.

Independent Component Analysis

All gray matter images were processed using spatial ICA [Calhoun et al., 2001] as implemented in the GIFT toolbox (http://icatb.sourceforge.net). ICA was performed using a neural network algorithm (infomax) that attempts to minimize the mutual information of the network outputs [Bell and Sejnowski, 1995; Lee et al., 1999]. Every gray matter image is converted into a one-dimensional vector. The 120 gray matter images of schizophrenia patients and 120 gray matter images of healthy controls were arrayed into one 240-row subject-by-gray matter data matrix. This matrix was then decomposed into mixing matrix and source matrix (see Fig. 3). The mixing matrix expresses the relationship between 240 subjects and k components. The rows of the matrix are scores which indicate to what degree that the k components contribute to a given subject. The columns of the matrix indicate how one component contributes to the 240 subjects. In contrast, the source matrix expresses the relationship between the k components and the voxels within the brain. The rows of the matrix indicate how one component contributes to different brain voxels, and the columns of the matrix are scores that indicate how one voxel contributes to each of the components.

Statistical Analysis

We used the mixing matrix for statistical analysis. Since every column of the mixing matrix contains the loading parameters expressing the contribution of every component to the 240 subjects, a two sample t-test can be used to

every column of the mixing matrix to test which components show a difference between healthy control and schizophrenia. A corrected threshold of $p < 0.05$ that controls for the false discovery rate was used as control for the number of components tested [Genovese et al., 2002].

The effects of age and sex on the significant sources were also determined. We regressed every columns of the mixing matrix separately on age and sex using a threshold of $p < 0.05$ to determine the sources that were significantly affected by age and sex. Then we did linear fitting to express the group differences versus age and sex. In order to verify that the group differences in the significant sources were still present after removing the effect of age and sex, we computed a two sample *t*-test on the residual of the regression and tested the difference between controls and patients.

Visualization

We used the source matrix for visualization. We reshaped every row of the source matrix back into a 3D image (source map). These source maps were scaled to unit standard deviation (SBM *Z* map) and thresholded at a value of $|Z| > 3.0$. The maps of the significant sources were then superimposed on the MNI-normalized template brain. The coordinates of the most significant sources were transformed from the MNI coordinate system to the coordinates of the standard space of Talairach and Tournoux [1988] using a Matlab conversion program written by Matthew Brett (http://imaging.mrc-cbu.cam.ac.uk/downloads/MNI2tal, MRC Cognition and Brain Sciences Unit, Cambridge, England). Once converted, the Talairach coordinates were entered into the Talairach Daemon [Lancaster et al., 2000] and summarized.

Comparison With VBM

We also analyzed the same sMRIs by the VBM approach. SPM5 was employed to do this analysis. The preprocessed images were directly entered into a two sample *t*-test to identify voxels that show a significant difference in gray matter concentration between healthy controls and patients with schizophrenia (*t* map). In order to perform a valid comparison with SBM, the VBM *t* map was converted to a *Z* map. Then the *Z* map was thresholded at a value of $|Z| > 3.0$ and visualized on the MNI template. For SBM, the two sample *t*-test on the mixing matrix was used to determine the significant sources. The SBM *Z* maps corresponding to the significant sources were then compared directly with the VBM *Z* map. Because the SBM and VBM maps are both converted to *Z* units, we can directly compare them.

RESULTS

Thirty-one components were estimated at the component estimation step. The mixing matrix and source matrix were estimated using ICA. We then analyzed the mixing matrix using a two-sample *t*-test for patients versus controls, with covariates included for sex and age. Nine sources whose loading scores differed significantly between controls and patients were identified. Upon visual inspection of the nine sources showing significant group differences, four sources were suggestive of obvious artifacts such as showing sharp edges, especially near the boundary of the brain or appearing primarily in regions that do not contain gray matter (e.g. white matter or ventricles). The remaining five sources contained areas where gray matter was greater in controls than in patients. The Talairach coordinates for these five sources are listed in Table I. There were some sources showing areas where gray matter was greater in patients versus control values, but the corresponding *p* values were not significant.

Anatomy of the Significant Sources

All of the five sources showed regions where gray matter concentrations were relatively greater in healthy controls than in schizophrenia patients. They are listed by the anatomical regions they represent in the order of increasing *p* values (decreasing significance).

Source 1: Bilateral Temporal

The largest gray matter difference between diagnostic groups was found in the region of the superior temporal gyrus (STG), with healthy controls having more gray matter than schizophrenia patients (see Fig. 4, red blob). These gray matter differences were notably constrained to the STG and its medial counterparts, the transverse temporal gyrus and insula, suggesting a clear distinction between these structures and the rest of the temporal lobe.

Source 2: Thalamus

The second source was localized bilaterally to the thalamus and hypothalamus, where less gray matter was also seen in cuneus and lingual gyrus in schizophrenia patients (see Fig. 4, green blob).

Source 3: Basal Ganglia

The third source was localized to the basal ganglia area and included the putamen, lateral and medial globus pallidus, and claustrum, with less gray matter in schizophrenia patients (see Fig. 4, blue blob).

Source 4: Parietal

This source consisted of bilateral parietal gray matter concentration that was greater in healthy controls than in schizophrenia patients. The gray matter differences were most marked in precuneus, superior parietal lobule, infe-

TABLE I. Talairach labels for regions of the five significant sources

	Brodmann area	L/R volume (cc)	L/R: max $Z(x, y, z)$
Source 1 area			
Superior temporal gyrus	22, 38, 41, 42, 13, 21	17.3/18.6	12.1(−45, 13, −8)/12.3(45, 3, −4)
Insula	13, 41, 40	8.4/11.2	9.0(−42, 8, −5)/13.7(45, 8, −5)
Inferior frontal gyrus	47, 45, 13, 9, 44	8.6/13.6	11.9(−42, 15, −12)/14.0(43, 13, −9)
Precentral gyrus	6, 44, 13, 43	2.8/2.4	10.0(−46, −9, 5)/4.9(53, 11, 6)
Anterior cingulate	32, 25, 24, 10	6.5/3.0	7.7(−1, 45, −2)/8.0(0, 45, 3)
Medial frontal gyrus	10, 11, 9, 32, 6, 8, 25	13.2/3.7	7.0(0, 51, 7)/7.2(0, 51, 2)
Transverse temporal gyrus	41, 42	1.9/2.2	6.7(−48, −17, 12)/7.2(43, −21, 12)
Thalamus		4.5/1.9	6.2(0, −17, 6)/4.5(4, −20, 9)
Postcentral gyrus	40, 43	1.9/1.3	5.9(−58, −21, 16)/6.1(59, −23, 14)
Uncus	34, 38, 28, amygdala	1.3/2.6	5.4(−27, 6, −20)/6.1(21, 5, −22)
Cingulate gyrus	32, 24	2.4/na	6.1(0, 35, 27)/na
Parahippocampal gyrus	34, 27, 30, 35, 28, amygdala	2.8/3.2	4.6(−15, 1, −16)/5.2(18, 2, −18)
Basal ganglia		1.3/2.8	3.8(−4, 13, −1)/5.1(37, −13, 5)
Superior frontal gyrus	9	0.4/na	4.8(−1, 52, 24)/na
Rectal gyrus	11	na/0.2	na/4.9(1, 34, −19)
Subcallosal gyrus	25, 34	0.9/0.4	4.3(−1, 8, −13)/3.7(4, 5, −10)
Middle temporal gyrus	21, 38	0.6/0.2	4.1(−52, −2, −11)/3.1(52, 2, −11)
Middle frontal gyrus	9, 46, 6, 8	na/0.9	na/4.0(48, 13, 30)
Inferior parietal lobule	40	0.2/0.9	3.9(−56, −28, 22)/4.0(52, −28, 21)
Orbital gyrus	11	0.2/na	3.7(0, 40, −21)/na
Source 2 area			
Thalamus		15.1/13.0	17.4(−10, −14, 10)/15.5(10, −16, 10)
Cuneus	17, 23, 18, 30, 7, 19	9.5/8.0	9.3(−7, −83, 6)/8.7(3, −83, 8)
Lingual gyrus	18, 17, 19	6.9/7.8	9.3(−1, −83, 4)/7.9(4, −81, 3)
Middle frontal gyrus	9, 46, 11	0.9/2.4	4.5(−36, 22, 31)/8.2(34, 17, 25)
Posterior cingulate	30, 31, 23	2.6/1.3	7.2(−7, −69, 12)/5.8(4, −68, 10)
Inferior parietal lobule	40	1.5/0.6	6.8(−36, −48, 40)/4.6(37, −55, 40)
Precuneus	31, 7, 23, 19	6.5/2.8	6.5(0, −69, 17)/6.8(4, −70, 21)
Middle and inferior occipital gyrus	18, 19	2.4/1.3	6.1(−19, −85, −5)/4.1(27, −78, 19)
Parahippocampal gyrus	30, 27, 36, 35, amygdala	0.6/1.9	4.8(−13, −31, −4)/4.2(18, −33, 0)
Supramarginal gyrus	40	0.4/na	4.6(−37, −42, 38)/na
Uncus	20, 28	na/0.9	na/4.4(27, −16, −29)
Cingulate gyrus	31, 24	0.4/na	4.3(−4, −60, 28)/na
Fusiform gyrus	19, 20	1.1/na	4.2(−21, −82, −10)/na
Superior temporal gyrus	39, 22	0.9/na	4.1(−48, −53, 12)/na
Medial frontal gyrus	6	1.3/0.2	4.0(−9, −18, 53)/3.1(7, −19, 59)
Middle and inferior temporal gyrus	11, 39	0.6/na	3.7(−39, −75, 11)/na
Postcentral gyrus	3, 1	na/1.1	na/4.0(30, −34, 46)
Basal ganglia		0.8/0.6	4.2(−12, −13, 21)/3.7(30, 5, −8)
Insula	13	na/0.4	na/3.3(36, 23, 18)
Inferior frontal gyrus	11	na/0.2	na/3.2(13, 34, −22)
Precentral gyrus	6, 4	na/0.4	na/3.1(45, −2, 43)
Source 3 area			
Lentiform nucleus		15.6/16.4	25.4(−27, 2, 3)/25.8(27, −1, 4)
Claustrum		7.6/5.0	18.8(−30, 6, 5)/15.1(33, −3, 2)
Insula	13	1.5/0.2	6.5(−33, 11, 8)/3.5(33, −1, 15)
Middle frontal gyrus	6, 8	1.7/2.8	4.9(−30, 17, 41)/6.2(28, 8, 42)
Subcallosal gyrus	34	0.2/0.2	5.9(−27, 2, −9)/3.0(27, 4, −9)
Cingulate gyrus	32	na/0.4	na/5.5(22, 8, 42)
Thalamus		1.3/5.2	3.7(−15, −23, 7)/5.2(18, −5, 13)
Caudate		1.1/0.9	4.9(−15, 11, 8)/5.2(15, 8, 9)
Parahippocampal gyrus	Amygdala	0.2/0.4	4.1(−25, −3, −10)/3.7(24, −6, −10)
Precuneus	7	na/0.4	na/3.6(25, −52, 40)
Precentral gyrus	9	0.2/na	3.5(−30, 21, 36)/na
Middle and superior temporal gyrus	39, 38	0.2/0.4	3.3(−40, 20, −31)/3.4(34, −58, 28)
Cuneus	18, 17	0.6/na	3.4(−18, −78, 20)/na
Medial frontal gyrus	9	na/0.2	na/3.2(25, 39, 17)
Middle occipital gyrus	18	na/0.2	na/3.1(18, −87, 13)
Inferior frontal gyrus	47	0.2/na	3.0(−40, 32, −4)/na
Fusiform gyrus	20	na/0.2	na/3.0(43, −11, −26)
Source 4 area			
Precuneus	7, 19, 31, 39	22.0/19.7	11.5(−1, −73, 45)/10.8(1, −70, 49)
Superior parietal lobule	7	11.9/12.7	10.6(−7, −67, 53)/10.3(6, −66, 54)

TABLE I. (continued)

	Brodmann area	L/R volume (cc)	L/R: max $Z(x, y, z)$
Inferior parietal lobule	7, 40, 39	11.9/9.1	8.0(−43, −56, 50)/8.6(39, −65, 47)
Postcentral gyrus	7, 5, 3, 40, 2	7.6/5.0	8.4(−21, −52, 65)/7.7(15, −52, 65)
Cuneus	19, 7, 30, 18	5.0/6.0	7.9(−1, −81, 37)/6.4(28, −80, 30)
Angular gyrus	39	2.2/1.5	6.0(−37, −76, 33)/5.1(43, −74, 31)
Superior occipital gyrus	19, 39	2.6/1.9	5.8(−34, −80, 28)/5.3(34, −80, 30)
Paracentral lobule	5	0.2/0.2	5.3(0, −46, 63)/3.2(7, −45, 59)
Middle and inferior temporal gyrus	19, 39	1.5/0.8	4.9(−37, −78, 23)/3.8(43, −74, 26)
Lingual gyrus	18	0.2/na	4.0(0, −68, 2)/na
Posterior cingulate	30, 29, 23	0.9/na	3.9(0, −62, 11)/na
Middle frontal gyrus	9, 6	0.4/na	3.9(−25, 33, 23)/na
Middle occipital gyrus	19	0.2/0.2	3.2(−37, −87, 18)/3.4(30, −85, 21)
Insula	13	na/0.4	na/3.3(45, −41, 21)
Parahippocampal gyrus	36	0.2/na	3.0(−30, −20, −29)/na
Source 5 Area			
Middle frontal gyrus	9, 10, 11, 46, 8, 47, 6	10.4/7.3	19.2(−34, 12, 28)/8.3(37, 15, 28)
Inferior frontal gyrus	9, 47, 46, 11	3.9/6.3	12.6(−34, 6, 29)/12.3(33, 10, 27)
Precentral gyrus	9, 6	2.4/3.0	11.9(−34, 12, 34)/10.4(34, 4, 29)
Superior temporal gyrus	13, 39, 38, 22, 41, 42, 21	7.6/10.6	6.2(−50, −40, 20)/9.8(43, −47, 22)
Insula	13	2.6/3.9	8.2(−45, −40, 20)/8.7(34, 17, 18)
Middle temporal gyrus	39, 21, 19, 22	4.1/1.7	7.5(−37, −69, 16)/5.2(49, −12, −12)
Inferior parietal lobule	40, 2	3.2/0.9	6.8(−45, −41, 26)/7.3(49, −47, 22)
Precuneus	31, 39	0.2/0.9	3.5(−39, −67, 31)/6.9(31, −73, 16)
Middle occipital gyrus	19, 18	1.9/2.4	5.8(−37, −75, 8)/6.1(34, −77, 12)
Anterior cingulate	10, 32, 24	9.5/7.1	6.0(−18, 47, −2)/5.3(3, 32, 4)
Medial frontal gyrus	6, 10, 25, 8, 9, 11	4.5/8.6	5.6(−15, 39, −10)/5.9(12, −6, 60)
Superior frontal gyrus	10, 11, 6, 9	2.2/4.8	5.6(−22, 48, 2)/4.8(15, −3, 64)
Supramarginal gyrus	40	1.3/0.9	5.5(−42, −45, 29)/5.4(43, −47, 30)
Cingulate gyrus	31, 32, 24	2.6/2.2	5.2(−13, −32, 38)/4.7(13, −27, 36)
Fusiform gyrus	20	0.4/0.9	3.6(−46, −7, −24)/5.0(42, −30, −14)
Posterior cingulate	30, 31	0.6/1.3	4.9(−31, −68, 17)/3.6(28, −68, 17)
Orbital gyrus	47	na/0.6	na/4.7(16, 27, −23)
Angular gyrus	39	0.4/na	4.5(−39, −59, 35)/na
Uncus	20, 28	0.6/na	4.5(−31, −16, −33)/na
Rectal gyrus	11	na/0.6	na/4.3(10, 18, −22)
Lingual gyrus	18	0.9/0.6	4.1(−15, −83, −2)/4.1(12, −77, −1)
Inferior temporal gyrus	20, 37	0.6/na	4.1(−46, −8, −19)/na
Postcentral gyrus	2, 5	0.9/0.2	3.8(−39, −24, 39)/3.8(33, −29, 40)
Basal ganglia		0.6/0.6	3.2(−12, 25, −4)/3.7(28, 18, 16)
Cuneus	18	na/0.4	na/3.6(10, −77, 27)
Inferior occipital gyrus	19	0.2/0.4	3.2(−37, −76, 0)/3.2(40, −83, −2)
Parahippocampal gyrus	30	0.2/na	3.0(−19, −48, 9)/na

Voxels above the threshold of $|Z| > 3.0$ were converted from Montreal Neurological Institute (MNI) coordinates to Talairach coordinates and entered into a database to provide anatomic and functional labels for the left (L) and right (R) hemispheres. The volume of voxels in each area is provided in cubic centimeters (cc). Within each area, the maximum Z value and its coordinate are provided.

rior parietal lobule (IPL), and postcentral gyrus (see Fig. 4, yellow blob).

Source 5: Frontal/Temporal

This source consisted of the bilateral middle frontal gyrus (along the border between gray matter and white matter), inferior frontal gyrus and medial frontal gyrus, plus portions of superior and middle temporal gyrus, anterior cingulate, and the temporoparietal junction (see Fig. 4, purple blob). The healthy controls had more gray matter than schizophrenia patients in this source.

Age and Sex Effect

There was no significant relationship of sex on any of the five sources. The effect of age on Sources 1 and 4 was significant. The correlation plots between age and ICA weights for Sources 1 and 4 are presented in Figure 5. The ICA weight (and hence gray matter concentration) decreased as age increased. The absolute value of the negative slope of the controls was slightly larger than that of the schizophrenia patients, although there was not a significant group difference in the slopes. The intercept of the controls was also slightly less than schizophrenia patients, again not signifi-

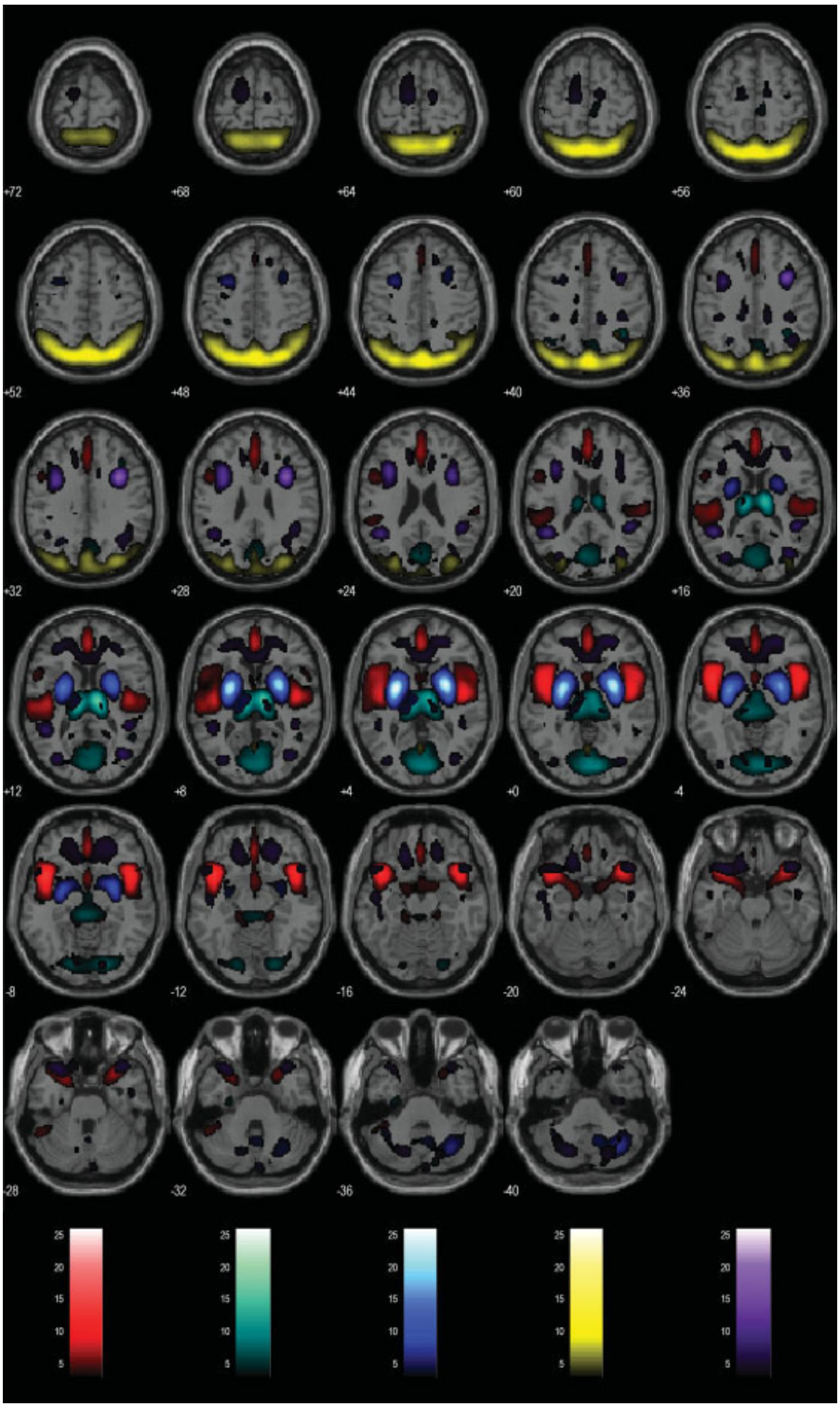

Figure 4.

Sources discovered by SBM. The voxels above the threshold of $|Z| > 3.0$ are shown. Red, bilateral temporal source; green, thalamus source; blue, basal ganglia source; yellow, parietal source; purple, frontal/temporal source.

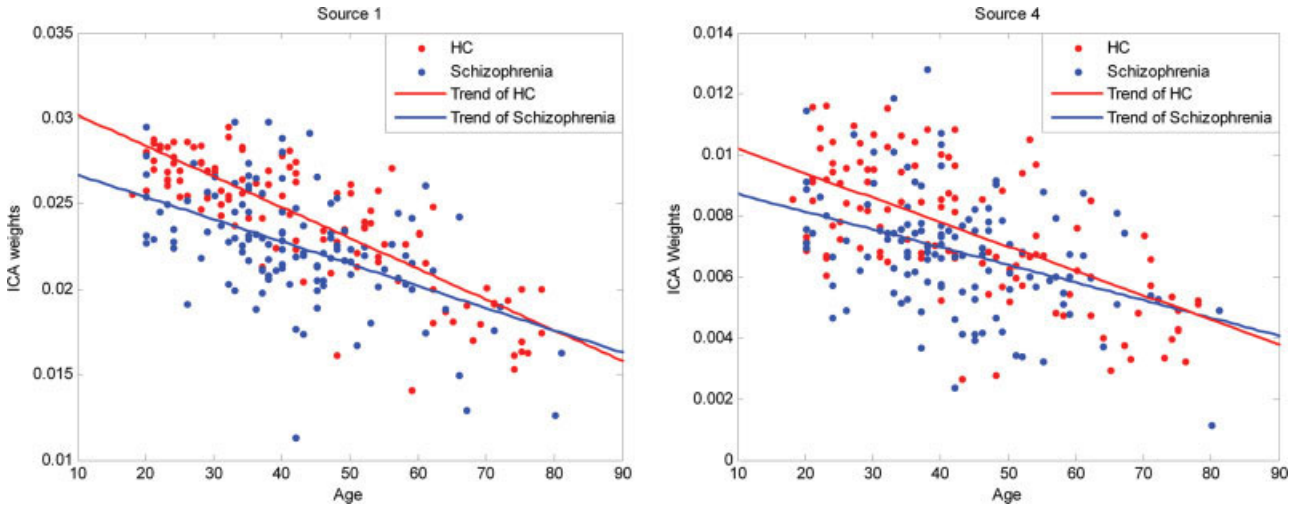

Figure 5.
The correlation plots between age and ICA weights for Sources 1 and 4. Left, the correlation for Source 1; right, the correlation for Source 4. Red dots, correlation for the controls; blue dots, correlation for the patients; red line, trend for red dots; blue line, trend for blue dots.

cantly. After removing the effect of age, the group differences in the sources remained unchanged, with the exception that the significance level for Source 4 increased.

VBM vs. SBM

In Figure 6 we present the voxels determined by VBM superimposed on a canonical gray matter image. Table II provides the Talairach table summaries of the VBM results, which reveal that the gray matter reduction in schizophrenia is significant in thalamus, basal ganglia, STG, and frontal gyrus. The identity of the regions found by SBM and VBM differed in size and intensity. Nearly all the regions found by VBM approach were also identified by SBM. The SBM approach showed more regions of difference in basal ganglia, parietal lobe, and occipital lobe, which did not appear in VBM. The most significant source found by SBM (based upon the *t*-test of the mixing parameters) was the STG, followed by thalamus, occipital lobule, basal ganglia, and frontal and parietal lobule. For VBM, the order (based upon the voxelwise *t*-values) was thalamus, followed by basal ganglia and frontal gyrus and temporal gyrus. Neither method found regions showing increases in gray matter concentration in schizophrenia versus healthy controls.

DISCUSSION

SBM Analysis

In this paper, we propose the use of ICA as an approach to decompose gray matter segmentation images into natural groups showing similar covariation between subjects. We define this approach as SBM. This approach can be considered a multivariate version of the commonly used VBM. We present an application of this approach to detect structural gray matter concentration differences between 120 healthy controls and 120 patients with schizophrenia. SBM successfully identified five sources that significantly differentiated the groups. All of the five sources corresponded to regions that showed higher gray matter concentration in healthy controls than patients with schizophrenia. Since the initialization of ICA is picked randomly by the infomax algorithm included in the GIFT tool box, we ran the SBM procedure several times to make sure that the results were consistent. A study of the consistency of several different ICA algorithms in the GIFT tool box can be found in Correa's paper [Correa et al., 2007]. We now provide a brief discussion of the results from the schizophrenia analysis, followed by a discussion of SBM and the differences between SBM and VBM.

Source 1, the most significant source region of gray matter disturbance, contains a large continuous region of temporal lobe that included the bilateral STG, transverse temporal gyrus, and insula, but not most of middle or inferior temporal regions. This is consistent with previous reports of selective reductions in the STG [Hirayasu et al., 2000; Mitelman et al., 2005; Pearlson, 1997].

Source 2 consisted of thalamic areas and hypothalamus, consistent with some previous work showing thalamic volume reductions in schizophrenia [Csernansky et al., 2004; Gaser et al., 2004]. The cuneus and lingual gyrus reductions agree with the occipital lobe volume reductions reported by others [Andreasen et al., 1994].

Source 3 showed gray matter differences in basal ganglia. This is consistent with reports of basal ganglia decrease [Corson et al., 1999] with the newer, atypical antipsychotic medications, although basal ganglia increases in

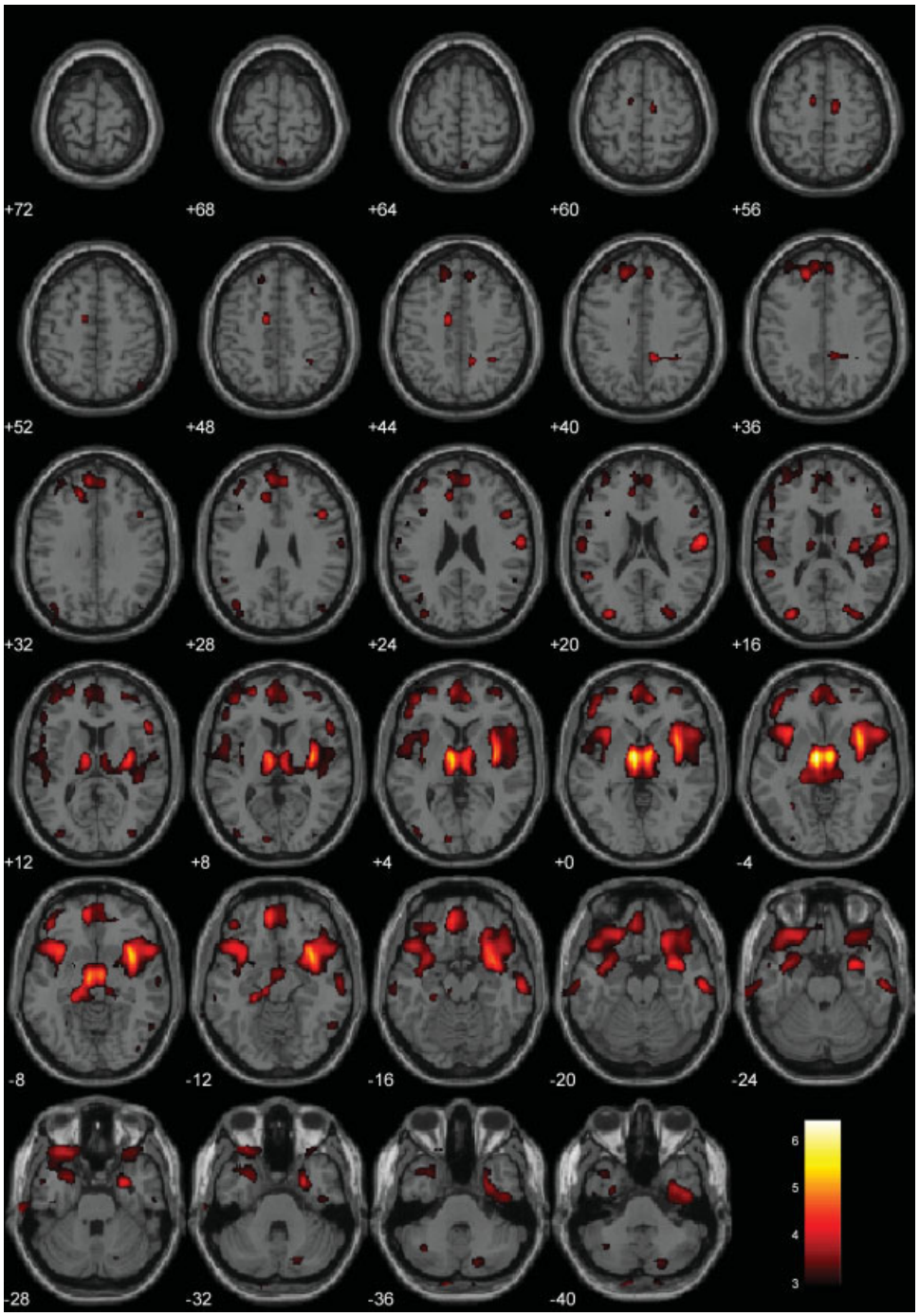

Figure 6.
Differences in gray matter concentration between healthy controls and schizophrenia delineated by VBM. The voxels above the threshold of $|Z| > 3.0$ are shown.

volume are well described as a side effect of treatment with first-generation antipsychotic medications [Hokama et al., 1995]. Reductions in claustrum were reported by Salgado-Pineda et al. [Salgado-Pineda et al., 2003].

Source 4 revealed that healthy controls had greater gray matter concentrations in precuneus, IPL, and superior parietal and postcentral gyrus. Although there have been a number of reports showing differences in the volumes of

TABLE II. Talairach labels for the result of VBM

VBM area	Brodmann area	L/R volume (cc)	L/R: max $Z(x, y, z)$
Thalamus		6.5/7.8	5.0(−6, −9, 2)/6.5(7, −9, −2)
Basal ganglia		7.7/4.4	5.4(−36, 6, −3)/4.1(34, 10, −2)
Inferior frontal gyrus	47, 13, 11, 45, 9, 10, 44, 46	13.8/14.0	5.2(−34, 16, −5)/4.4(40, 17, −8)
Insula	13, 40	6.3/3.2	4.9(−34, 12, −1)/4.7(34, 14, −6)
Superior temporal gyrus	38, 22, 13, 41, 39, 21	12.5/11.2	4.8(−36, 2, −13)/3.9(33, 1, −18)
Medial frontal gyrus	11, 10, 6, 9, 8	8.9/9.3	4.0(−12, −8, 53)/4.7(7, 46, −14)
Parahippocampal gyrus	34, 27, amygdala, 36, 35, 19, 30, 28	1.7/2.4	4.7(−30, 4, −14)/4.1(21, −31, −6)
Postcentral gyrus	43, 3, 40, 7	2.8/1.3	4.7(−58, −9, 18)/3.6(56, −14, 17)
Inferior temporal gyrus	20, 21, 37	5.6/1.7	4.3(−61, −20, −15)/3.5(62, −18, −17)
Uncus	Amygdala, 28, 20, 36, 38	3.7/2.6	4.3(−28, 0, −21)/3.7(30, −8, −36)
Middle occipital gyrus	19, 18	0.9/1.5	3.7(−28, −78, 20)/4.3(31, −79, 21)
Middle frontal gyrus	11, 46, 47, 10, 9, 8	4.8/10.4	4.2(−25, 25, −18)/3.9(43, 39, −10)
Cingulate gyrus	24, 31, 32	1.1/1.7	4.0(−12, −42, 39)/4.2(12, −4, 43)
Superior frontal gyrus	9, 10, 8, 11	1.5/8.9	3.3(−30, 55, −4)/4.1(16, 38, 31)
Anterior cingulate	10, 32, 25, 24	2.4/2.4	4.0(−9, 48, −2)/3.7(10, 35, 20)
Middle temporal gyrus	21, 39, 19	4.3/2.6	3.9(−64, −22, −11)/3.5(40, −68, 30)
Precentral gyrus	4, 44, 6, 43, 9	2.4/1.5	3.8(−59, −4, 17)/3.4(49, 11, 6)
Precuneus	31, 7, 19	1.9/1.1	3.8(−22, −73, 19)/3.5(27, −76, 18)
Inferior parietal lobule	40, 7	0.9/0.6	3.7(−33, −43, 44)/3.5(53, −44, 26)
Orbital gyrus	47, 11	0.2/1.9	3.1(−3, 41, −20)/3.7(19, 32, −22)
Cuneus	17, 18	na/0.4	na/3.6(10, −87, 10)
Rectal gyrus	11	na/0.4	na/3.5(9, 38, −20)
Transverse temporal gyrus	41, 42	0.4/1.1	3.5(−42, −30, 13)/3.2(62, −11, 14)
Superior occipital gyrus	19	0.2/1.5	3.1(−30, −83, 22)/3.4(33, −79, 26)
Angular gyrus	39	0.2/0.2	3.0(−46, −71, 33)/3.3(39, −74, 31)
Inferior occipital gyrus	19, 18	0.2/0.2	3.2(−40, −80, −4)/3.0(33, −82, −3)
Subcallosal gyrus	34	na/0.2	na/3.2(25, 5, −12)
Supramarginal gyrus	40	0.4/0.2	3.1(−55, −45, 23)/3.0(49, −47, 29)
Superior parietal lobule	7	0.4/na	3.1(−42, −64, 54)/na
Fusiform gyrus	20, 37	0.4/na	3.1(−56, −17, −23)/na

Voxels above the threshold of $|Z| > 3.0$ were converted from Montreal Neurological Institute (MNI) coordinates to Talairach coordinates and entered into a database to provide anatomic and functional labels for the left (L) and right (R) hemispheres. The volume of voxels in each area is provided in cubic centimeters (cc). Within each area, the maximum Z value and its coordinate are provided.

IPL, superior parietal region, and postcentral gyrus [Frederikse et al., 2000; Shenton et al., 2001], our findings suggested that, in addition, the precuneus, which has not been well studied, might also be a key area in the regional brain abnormalities which underlie the disease.

Source 5 showing gray matter deficits in schizophrenia in the middle frontal and inferior frontal gyri was consistent with prior reports [Buchanan et al., 1998; Goldstein et al., 1999; Gur et al., 2000] and replicated Mitelman's reports of differing intercorrelations of prefrontal and temporal volumes between patients and controls [Mitelman et al., 2005].

Every source reveals a set of regions that are significantly different between the two diagnoses. Although most regions identified in different sources implicate regional difference of particular brain areas, examination of the Talairach tables reveals overlap in several sources. Indeed, the overlapping regions appear to underlie aspects of higher cortical function such as language and executive function that appear to be most disturbed in schizophrenia patients. The thalamus is a major relay station in the brain and deals with inputs from many other brain regions. The executive function makes it not surprised to identify some parts of thalamus in Sources 1, 2, and 3. As a part of the multifunctional basal ganglia, the caudate nucleus was identified in Sources 1, 2, and 5. The insula was seen in all sources, implying its role of various highly conserved functions. In addition, the posterior cingulate cortex (BA 30, 31, 23, and 29) found in Sources 2, 4, and 5, mesial temporal regions including the uncus found in Sources 1, 2, and 5, and the parahippocampal gyrus identified in Sources 1, 2, 3, 4, and 5 are frequently found to be structurally altered in individuals with schizophrenia.

More interestingly, some of these overlapping regions are likely normally highly reciprocally interconnected (this could be tested in follow-up studies using more direct measures of connectivity, e.g. diffusion tensor imaging data). For example, the dorsolateral prefrontal cortex (BA 9 and 46) that appears in Sources 1, 2, and 5, the STG (BA 22, 39, 41, and 42) identified in Sources 1, 2, 3, and 5, and IPL (BA 39 and 40) seen in Sources 1, 2, 4, and 5 are connected to the anterior cingulate cortex (BA 24, 31, 32) implicated in Sources 1, 2, 3, and 5. These comprise the most important core nodes in the heteromodal association cortical circuit [Pearlson et al., 1996; Ross and Pearlson, 1996].

We found no sex effect on any source, and significant age effects were only for Sources 1 and 4. The negative

slopes of the correlations between ICA weights and age of both the healthy control and schizophrenia for these two sources reveals that their volumes decreased with the age in both diagnostic groups. The absolute value of the slope for healthy controls was higher than patients while the intercept was lower for controls than patients for both sources, suggesting that the source volumes in patients decrease at an early age and continue declining with increasing age. By age 75, the source volumes reached a similar size for both schizophrenia and healthy controls. For Sources 1 and 4, we noted the reduction of STG [Keshavan et al., 1998] and parietal lobe respectively with age for schizophrenia.

In summary, SBM identified five sources (groups of regions that covary in a particular manner from individual to individual). An advantage of the SBM approach is it incorporates the additional information about the grouping of the regions within several distinct, anatomically consistent sources. This contrasts with VBM, which identifies a large set of regions but does not recognize relationships among them. We now provide a comparison of SBM and VBM.

SBM vs VBM: Strengths and Limitations

Because SBM is a multivariate approach, it can take into account the interrelationship between voxels in order to identify naturally grouped regions. The sources revealed by SBM provide information about the localization of gray matter changes. The mixing matrix columns containing the linear combinations of the sources provide information about the pathological and normal variation among individuals. Through the mixing matrix, the contribution of individual brain variations to the sources can be clearly represented. An additional benefit of our approach is that SBM can remove sources that exhibit obvious artifactual patterns, and thus we are in effect performing a spatial filtering of the results (see Fig. 2 and simulation). In summary, we have shown that SBM can result in less-noisy sources of interest, enable examination of their association with subject variables (such as diagnosis or age), and provide information about the interrelationship between the sources because of its multivariate nature. While VBM is a powerful and easy approach to implement, its results do not provide information about how regions identified are related to one another. VBM also does not incorporate spatial filtering, and our empirical VBM results appeared generally noisier. Therefore, SBM is a useful method for identifying regions exhibiting similar underlying covariation in gray matter among subjects and can be considered a multivariate complement to VBM, with the specific advantages discussed earlier.

CONCLUSION

The use of SBM allowed us to identify the source networks showing significant differences between schizophrenia and healthy controls. Each identified source represents a distinct set of regions derived from the dataset. Our approach provides at least three distinct advantages over VBM. First, SBM allows noise reduction of the results by spatially filtering artifactual sources. Second, SBM is a multivariate method that takes the interrelationship among voxels into account. Third, SBM estimates the mixing matrix parameters that captures the covariation of specific sources among individuals. Specifically, the mixing matrix parameters allow the identification of sources that exhibit group differences or particular relationships with other variables of interest (e.g. age and sex). In addition, because the SBM statistical tests are performed on a small set of sources, instead of on each voxel as in VBM, it offers the additional benefit of minimizing the number of comparisons. SBM is particularly well suited for capturing natural constellations of brain volumes within groups of subjects that may reflect valid sets of regions. The application of SBM to structural brain images thus creates new opportunities to identify distinct brain source networks between groups.

ACKNOWLEDGMENTS

We thank Nicole Giuliani for her efforts in preprocessing the VBM data and for providing other helpful input, and Abigail Garrity for help with the manuscript text.

REFERENCES

Akaike H (1974): A new look at statistial nodel identification. IEEE Trans Autom Control 19:716–723.

Andreasen NC, Flashman L, et al. (1994): Regional brain abnormalities in schizophrenia measured with magnetic resonance imaging. JAMA 272:1763–1769.

Ashburner J, Friston K (1997): Multimodal image coregistration and partitioning—A unified framework. Neuroimage 6:209–217.

Ashburner J, Friston KJ (2000): Voxel-based morphometry—The methods. Neuroimage 11(6, Part 1):805–821.

Bell AJ, Sejnowski TJ (1995): An information-maximization approach to blind separation and blind deconvolution. Neur Comput 7:1129–1159.

Buchanan RW, Vladar K, et al. (1998): Structural evaluation of the prefrontal cortex in schizophrenia. Am J Psychiatry 155:1049–1055.

Calhoun VD, Adali T (2006): 'Unmixing' functional magnetic resonance imaging with independent component analysis. IEEE Eng Med Biol 25:79–90.

Calhoun VD, Adali T, et al. (2001): A method for making group inferences from functional MRI data using independent component analysis. Hum Brain Mapp 14:140–151.

Correa N, Adali T, et al. (2007): Performance of blind source separation algorithms for fMRI analysis using a group ICA method. Magn Reson Imaging 25:684–694.

Corson PW, Nopoulos P, et al. (1999): Change in basal ganglia volume over 2 years in patients with schizophrenia: Typical versus atypical neuroleptics. Am J Psychiatry 156:1200–1204.

Csernansky JG, Schindler MK, et al. (2004): Abnormalities of thalamic volume and shape in schizophrenia. Am J Psychiatry 161:896–902.

First MB, Spitzer RL, et al. (1997). Structured Clinical Interview for DSM-IV Axis I Disorders—Clinical Version (SCID-IV). Washington, DC: American Psychiatric Press.

Frederikse M, Lu A, et al. (2000): Sex differences in inferior parietal lobule volume in schizophrenia. Am J Psychiatry 157:422–427.

Gaser C, Nenadic I, et al. (2004): Ventricular enlargement in schizophrenia related to volume reduction of the thalamus, striatum, and superior temporal cortex. Am J Psychiatry 161:154–156.

Genovese RC, Lazar AN, et al. (2002): Thresholding of statistical maps in functional neuroimaging using the false discovery rate. Neuroimage 15:870–878.

Goldstein JM, Goodman JM, et al. (1999): Cortical abnormalities in schizophrenia identified by structural magnetic resonance imaging. Arch Gen Psychiatry 56:537–547.

Good CD, Johnsrude IS, et al. (2001): A voxel-based morphometric study of ageing in 465 normal adult human brains. Neuroimage 14(1, Part 1):21–36.

Gur RE, Cowell PE, et al. (2000): Reduced dorsal and orbital prefrontal gray matter volumes in schizophrenia [erratum appears in Arch Gen Psychiatry 2000;57:858]. Arch Gen Psychiatry 57:761–768.

Hirayasu Y, McCarley RW, et al. (2000): Planum temporale and Heschl gyrus volume reduction in schizophrenia: A magnetic resonance imaging study of first-episode patients. Arch Gen Psychiatry 57:692–699.

Hokama H, Shenton ME, et al. (1995): Caudate, putamen, and globus pallidus volume in schizophrenia: A quantitative MRI study. Psychiatry Res 61:209–229.

Karhunen J, Cichocki A, et al. (1997): On neural blind separaton with noise suppression and redundancy reduction. Int J Neural Syst 8:219–237.

Keshavan MS, Haas GL, et al. (1998): Superior temporal gyrus and the course of early schizophrenia: Progressive, static, or reversible? J Psychiatry Res 32:161–167.

Lancaster JL, Woldorff MG, et al. (2000): Automated Talairach atlas labels for functional brain mapping. Hum Brain Mapp 10:120–131.

Lee T-W., Girolami M, et al. (1999): Independent component analysis using an extended infomax algorithm for mixed subgaussian and supergaussian sources. Neur Comput 11:417–441.

Li YO, Adali T, et al. (2007): Estimating the number of independent components for functional magnetic resonance imaging data. Hum Brain Mapp 28:1251–1266.

Makeig S, Jung T, et al. (1997): Blind separation of auditory event-related brain responses into independent components. Proc Natl Acad Sci USA 94:10979–10984.

Mitelman SA, Shihabuddin L, et al. (2005): Cortical intercorrelations of temporal area volumes in schizophrenia. Schizophrenia Res 76:207–229.

Nakai T, Muraki S, et al. (2004): Application of independent component analysis to magnetic resonance imaging for enhancing the contrast of gray and white matter. Neuroimage 21:251–260.

Pearlson GD (1997): Superior temporal gyrus and planum temporale in schizophrenia: A selective review. Prog Neuropsychopharmacol Biol Psychiatry 21:1203–1229.

Pearlson GD, Marsh L (1999): Structural brain imaging in schizophrenia: A selective review. Biol Psychiatry 46:627–649.

Pearlson GD, Petty RG, et al. (1996): Schizophrenia: A disease of heteromodal association cortex? Neuropsychopharmacology 14:1–17.

Ross CA, Pearlson GD (1996): Schizophrenia, the heteromodal association neocortex and development: Potential for a neurogenetic approach. Trends Neurosci 19:171–176.

Salgado-Pineda P, Baeza I, et al. (2003): Sustained attention impairment correlates to gray matter decreases in first episode neuroleptic-naive schizophrenic patients. Neuroimage 19(2, Part 1):365–375.

Shenton ME, Dickey CC, et al. (2001): A review of MRI findings in schizophrenia. Schizophrenia Res 49:1–52.

Spitzer RL, Williams JBW, et al. (1989): Structured Clinical Interview for DSM-III-R-Patient Version (SCID-P, 5/1/89). New York, NY: New York State Psychiatric Institute.

Talairach J, Tournoux P (1988): Co-Planar Stereotactic Atlas of the Human Brain: 3-Dimensional Proportional System—An Approach to Cerebral Imaging. New York, NY: Thieme Medical Publishers.

Wax M, Kailath T (1985): Detection of signals by information theoretic criteria. IEEE Trans Acoust Speech Sig Proc 33:387–392.